Atmosphere–Ocean Interaction in the North Atlantic: Near-Surface Climate Variability*

Uma S. Bhatt

Department of Atmospheric and Oceanic Sciences, University of Wisconsin—Madison, Madison, Wisconsin

Michael A. Alexander

CIRES, University of Colorado, Boulder, Colorado

David S. Battisti

Department of Atmospheric Sciences, University of Washington, Seattle, Washington

David D. Houghton and Linda M. Keller

Department of Atmospheric and Oceanic Sciences, University of Wisconsin—Madison, Madison, Wisconsin

(Manuscript received 27 January 1997, in final form 22 August 1997)

ABSTRACT

The impact of an interactive ocean on the midlatitude atmosphere is examined using a 31-yr integration of a variable depth mixed layer ocean model of the North Atlantic (between 20° and 60°N) coupled to the NCAR Community Climate model (CCM1). Coupled model results are compared with a 31-yr control simulation where the annual cycle of sea surface temperatures is prescribed. The analysis focuses on the northern fall and winter months.

Coupling does not change the mean wintertime model climatology (December–February); however, it does have a significant impact on model variance. Air temperature and mixing ratio variance increase while total surface heat flux variance decreases. In addition, it is found that air–sea interaction has a greater impact on seasonally averaged variance than monthly variance.

There is an enhancement in the persistence of air temperature anomalies on interannual timescales as a result of coupling. In the North Atlantic sector, surface air and ocean temperature anomalies during late winter are uncorrelated with the following summer but are significantly correlated (0.4–0.6) with anomalies during the following winter. These autocorrelations are consistent with the ''re-emergence'' mechanism, where late winter ocean temperature anomalies are sequestered beneath the shallow summer mixed layer and are reincorporated into the deepening fall mixed layer. The elimination of temperature anomalies from below the mixed layer in a series of uncoupled sensitivity experiments notably reduces the persistence of year-to-year anomalies.

The persistence of air temperature anomalies on monthly timescales also increases with coupling and is likely associated with ''decreased thermal damping.'' When coupled to the atmosphere, the ocean is able to adjust to the overlying atmosphere so that the negative feedback associated with anomalous heat fluxes decreases, and air temperature anomalies decay more slowly.

1. Introduction

The prominent mode of observed interannual wintertime air and ocean temperature variability in the North Atlantic is characterized by anomalies of one sign in the north (35°–60°N) and of opposite sign in the south (20°–35°N). The associated atmospheric circulation anomalies in sea level pressure (SLP) and 500-mb heights, commonly known as the west Atlantic pattern (Wallace and Jiang 1987), is equivalent barotropic and displays a trough centered to the north of a cold northern SST anomaly center and a ridge over a warm southern SST anomaly (Wallace and Jiang 1987; Wallace et al. 1990; Wallace et al. 1992). Patterns of interannual variability closely resembling the observations have been documented in atmospheric general circulation models integrated with fixed SSTs (Delworth 1996; Bhatt 1996; Bladé 1997; Saravanan 1998) and will be found in this study.

Observational as well as modeling studies suggest that coupled ocean–atmosphere variability on interan-

nual timescales (less than approximately 10 yr) is controlled primarily by local interactions that occur through surface heat flux anomalies. Bjerknes (1962, 1964) first described the dipolelike anomaly pattern and demonstrated that North Atlantic sea surface temperature (SST) anomalies on interannual timescales are negatively correlated with local wind speed and result from anomalous local air–sea heat fluxes. Recent investigations (Deser and Blackmon 1993; Kushnir 1994) using the Comprehensive Ocean and Atmosphere Data Set (COADS) spanning most of this century confirm and expand upon the findings of Bjerknes. Frankignoul and Reynolds (1983) demonstrated that fluctuations of observed estimates of anomalous surface heat fluxes are larger than oceanic heat flux convergence due to anomalous Ekman advection. This lead them to conclude that surface heat fluxes are the dominant forcing of oceanic anomalies on interannual timescales. Haney (1985) and Battisti et al. (1995) forced ocean models with observed anomalous surface conditions in the midlatitude Pacific and Atlantic Oceans, respectively, and concluded that surface heat flux forcing can explain most of the interannual oceanic variability. Changes in SST due to ocean dynamics (advection) have been shown to be important for longer timescales (decadal or more) (Luksch 1996; Delworth 1996) than are of interest here.

The observations indicate that large-scale atmospheric anomalies lead corresponding anomalies in the ocean. The large-scale atmospheric anomalies in sea level pressure (Zorita et al. 1992) and 500-mb heights (Wallace and Jiang 1987) lead the dipole anomalies in the ocean, consistent with the atmosphere initially forcing the ocean. Cayan (1992) extensively examined the relationship between surface heat fluxes and SST anomalies using observations and found significant correlations between surface heat flux and wintertime extratropical ocean temperature tendency suggesting that the atmosphere forces the large-scale midlatitude SST anomalies.

Modeling studies have examined the response of the atmosphere to midlatitude SST anomalies with varying results. Some researchers find a distinct atmospheric response downstream consistent with the sign of the imposed SSTs (e.g., Palmer and Sun 1985; Peng et al. 1995; Ferranti et al. 1994), whereas others studies do not (e.g., Pitcher et al. 1988; Kushnir and Lau 1992). Model resolution aside, it is possible that the atmospheric model response to fixed observed SST anomalies may depend on the location of the SST anomaly in relation to the atmospheric model climatology (Peng et al. 1997).

Observations alone are not sufficient to examine cause and effect relationships in the coupled climate system. Since, to the first order, the atmosphere forces the ocean in the midlatitudes, climate experiments that specify SST anomalies may not be ideal for studying the impact of the ocean on the atmosphere. Recently, coupled simulations have documented more subtle effects of the ocean on the atmosphere, namely an increase in the variance and persistence of lower-atmospheric anomalies. Lau and Nath (1996) demonstrate, using the Geophysical Fluids Dynamics Laboratory (GFDL) atmospheric model and a fixed-depth mixed layer ocean model, that the near-surface atmospheric anomalies increase significantly with coupling. Amplification of variance as a result of coupled ocean–atmosphere interactions has also been documented by Gallimore (1995) and Manabe and Stouffer (1996).

Barsugli (1995) examined the "increased variance" and "enhanced persistence" of climate anomalies using a 50-m slab global ocean coupled to a two-level global GCM. He found that components of the natural uncoupled atmospheric variability are enhanced by an interactive ocean because the ocean–atmosphere interaction leads to reduced damping of thermal anomalies. When the ocean is able to adjust to the overlying atmosphere, then the negative feedback associated with anomalous surface energy flux is reduced, hence the term "decreased thermal damping." Bladé (1997) examines this mechanism further using the GFDL climate model coupled to a slab mixed-layer ocean in the midlatitudes and also found significant increases in the variance of the lower-tropospheric thermal field. Saravan (1998) also found a decrease in thermal damping with coupling in a study that compared the National Center for Atmospheric Research (NCAR) Climate System Model with companion uncoupled simulations of Community Climate Model version 3 (CCM3).

The observed tendency for SST anomalies to recur from one winter to the next without persisting through the intervening summer (Namias and Born 1970, 1974) can also have an impact on the persistence of thermal anomalies in the lower troposphere. Thermodynamic heat exchange occurs through surface fluxes with the overlying atmosphere and from heat exchange with ocean water from below the seasonal thermocline through entrainment (Frankignoul and Reynolds 1983; Alexander 1990a; Alexander and Deser 1995). The mixed layer is shallow throughout the summer and deepens during the fall, reaching a maximum depth during the winter. Entrainment has its maximum impact on SSTs during fall when the mean entrainment rate and the mean vertical ocean temperature gradient are relatively large. Namias and Born (1970, 1974) proposed a mechanism, termed "re-emergence" by Alexander and Deser (1995), to explain the correlation between SST anomalies from one winter to the next in the observations. Late winter surface ocean temperature anomalies that exist through a large depth of the ocean are sequestered below the shallow stable summer mixed layer. In the subsequent fall months, as the mixed layer deepens, the temperature anomalies from the previous winter are reincorporated into the mixed layer. This mechanism has been documented in ocean weathership data and explored using a mixed layer model by Alexander and Deser (1995).

In this study we go beyond previous modeling ap-

proaches by using a variable depth mixed layer model of the North Atlantic coupled to a global general circulation model with a seasonal cycle to examine the impact of the ocean on the atmospheric surface temperature variability in the midlatitude North Atlantic sector. The analysis focuses on the dominant mode of variability during northern winter and examines the role re-emergence and decreased thermal damping play in increasing the variance and persistence of near-surface climate anomalies. We find that enhanced variance and increased persistence of SST anomalies can in part be explained by the re-emergence mechanism. Our results also illustrate the important effects of decreased thermal damping that are documented in Barsugli (1995) and explained in Barsugli and Battisti (1998).

In this paper, section 2 describes the models and experiment design. Enhanced persistence and changes in variance due to coupling are documented in section 3 and examined in more detail in section 4. The summary is presented in section 5.

2. Models and experiment design

Sea surface temperature (SST) anomalies in the North Atlantic on interannual timescales are primarily associated with local atmosphere–ocean coupling and mixed layer physics. There is heat exchange through surface fluxes with the overlying atmosphere and through entrainment of water from below the thermocline into the surface mixed layer. Therefore, an ocean model with explicit mixed layer physics and no ocean dynamics is employed to represent the North Atlantic. The ocean model grid is composed of 89 horizontally independent column models of the upper ocean, which are aligned with the NCAR Community Climate Model (R15) grid between 20°N and 60°N in the Atlantic at an approximate resolution of 4.5° lat × 7.5° long.

a. Mixed layer ocean model

The near-surface layer of much of the world's oceans is vertically well mixed with nearly uniform temperature and salinity. A one-dimensional ocean model developed by Gaspar (1988), which has been formulated with climate simulations in mind, is used to represent the influence of surface forcing and entrainment on the temperature and depth of the mixed layer. The temperature tendency of the mixed layer is controlled by the net surface energy flux, penetrating solar radiation, entrainment, and diffusion:

$$\frac{\partial T_m}{\partial t} = \frac{(Q_{tot} - Q_{swh})}{\rho_0 C_P h} - \frac{W_e(T_m - T_b)}{h} + \left.\frac{\nu_H}{h}\frac{\partial T_m}{\partial z}\right|_{z=h},$$ (1)

where T_m is the mixed layer temperature, T_b the temperature just below the mixed layer, W_e the entrainment rate, ρ_0 the density of seawater, C_P the specific heat of ocean water, h the mixed layer depth, Q_{tot} the total surface energy flux into the ocean, Q_{swh} the penetrating solar radiation at h, ν_H the molecular diffusion coefficient for heat, and z the vertical coordinate (positive downward). The entrainment rate is derived by vertically integrating the turbulent kinetic energy equation over the depth of the mixed layer and then parameterizing the resulting terms using the known variables [see Eq. (A9) in Battisti et al. 1995]. The salinity tendency of the mixed layer is described by an equation similar to Eq. (1) with the exception that the heat flux forcing in the first term is replaced with evaporation minus precipitation [see Eq. (A2) in Battisti et al. 1995].

The mixed layer depth increases via entrainment, which depends on the surface buoyancy forcing, wind stress, and penetrating solar radiation. The entrainment equation [see Eq. (50) in Gaspar 1988] has several adjustable parameters; we have used Gaspar's estimates of these time-independent parameters in all of our simulations. When deepening, h is computed as a prognostic variable; when shoaling, the mixed layer re-forms closer to the surface, entrainment is set to zero, and h is computed as a diagnostic quantity by assuming a balance between wind stirring and surface buoyancy forcing. When the mixed layer shoals, the temperature profile is adjusted according to Adamec et al. (1981), conserving both heat and potential energy.

The second term of the predictive equation for ocean temperature [Eq. (1)] from the mixed layer model (MLM) represents the net effect of heating at the surface and from below the mixed layer. The heating due to entrainment (Q_{we}) is given by

$$Q_{we} = -W_e(T_m - T_b)\rho_0 C_P,$$ (2)

where the variables are defined above. The magnitude of entrainment rate (W_e) is inversely proportional to the temperature jump at the base of the mixed layer (all other things being equal), with stronger entrainment rate associated with a smaller temperature difference between the mixed layer and the sub–mixed layer.

The region beneath the mixed layer is represented by a multilayer system where heat is redistributed through convective overturning, vertical diffusion, and penetrating solar radiation. The vertical diffusion is calculated using a constant coefficient of 2×10^{-5} m² s⁻¹ based on the study of White and Walker (1974). The absorption of solar radiation is parameterized following Paulson and Simpson (1977). The model contains 30 unequally spaced layers between the surface and 1000 m; 15 of the layers are within the first 100 m in order to adequately resolve the summer thermocline. The temperature of layers that are entirely above h are set to T_m, and T_b is obtained directly for

the layer in which h resides. The mixed layer model is described in more detail in Battisti et al. (1995).

b. Atmospheric model

The NCAR Community Climate Model version 1 (hereafter CCM1) is a sigma coordinate primitive equation GCM and serves as the atmospheric component in the modeling experiments. The CCM1 is a global spectral model with 12 layers in the vertical and rhomboidal 15 (R15) truncation resulting in a horizontal resolution in the transform grid of approximately 4.5° lat × 7.5° long. The formulation of radiation and cloudiness is discussed in Kiehl et al. (1987). Processes parameterized in the model include radiative transfer, moist and dry convective transports, subgrid-scale diffusive transports, and surface energy exchanges. CCM1 surface sensible and latent heat fluxes are calculated using a bulk parameterization, where the transfer coefficients depend on atmospheric static stability and wind speed (Deardorff 1972).

c. Experiment design and data processing

In the fully coupled simulation (COU), the ocean model is coupled to the NCAR CCM1 from 20° to 60°N in the North Atlantic and is integrated beginning on the first of January for 35 ⅓ yr. The remaining ocean SSTs and the global sea ice are specified according to the repeated annual cycle of the Alexander and Mobley (1976) climatology. The MLM is forced with heat, momentum, and freshwater fluxes from CCM1 in the coupled integration, where the ocean and atmosphere models are fully interactive. The integration time step is 30 min for CCM1 and 12 h for the MLM. Information is exchanged between the ocean and atmosphere every 12 h. Surface fluxes from CCM1 are averaged over 12 h and serve as the upper boundary condition of the MLM. Heat and salt flux corrections are added each day to the total heat and freshwater fluxes, respectively. The flux corrections are different at each ocean grid point and vary in time with a fixed annual cycle. A detailed discussion of the flux correction calculation and the patterns pertaining to this study is given in Battisti et al. (1995). Note that in the coupled model, flux corrections are used to bring the average ocean model SSTs close to climatological values when the MLM is forced with prescribed model atmospheric variables. The first 4 ⅓ yr of the simulation are not used in the analysis to ensure the models reach an equilibrium. The initial conditions for ocean temperature, salinity, and mixed layer depth are taken from the end state of a multiyear one-way forced integration where the MLM is forced by the CCM1 net surface flux.

The control simulation is integrated for 32 ⅓ yr using a specified annual cycle of global ocean surface temperatures and sea ice with no interannual variability.

The ocean model does not operate in the control simulation. The sea surface temperature climatology in the control simulation is prescribed as the long-term mean of the coupled simulation in all of the ocean basins.[1] The ocean temperature climatology in the oceanic regions other than the North Atlantic is from Alexander and Mobley (1976) for both the control and coupled simulations. The first 1 ⅓ yr of the control simulation are not included in the analysis.

Long-term monthly means of the model fields are calculated by averaging the 31-monthly values. Monthly anomalies are constructed by subtracting the long-term mean for a given month from the monthly mean during individual model years. Ocean temperature and mixed layer depth were not detrended. The analysis focuses on seasonal averages over the fall and winter seasons of the year, defined as the average over September–November and December–February (DJF), respectively. Observed surface variables over the North Atlantic Ocean from the Comprehensive Ocean Atmosphere Data Set (COADS) for the period 1950–88 are used in this study for evaluating the model results.

Sensitivity experiments that examine the impact of anomalies in entrainment, sub–mixed layer temperatures, and mixed layer depth on the persistence of the mixed layer temperature anomalies are presented in section 4. In these experiments the MLM is forced with heat and freshwater fluxes from the coupled simulation with no feedback to the atmospheric model, termed "one-way forced" following Alexander (1990b).

3. Results

a. Winter mean circulation

Difference maps for the mean climatologies of the control and coupled models are constructed by subtracting the long-term mean of the control from that of the coupled simulation for each field. Statistical significance is assessed on a point-by-point basis using the Student's t-test for significantly different means (Press et al. 1990).

The seasonal mean wintertime (DJF) surface heat fluxes, precipitation, sea level pressure, air temperature, mixing ratio, and winds over the North Atlantic from the control and the coupled simulations are not significantly different. Differences significant at the 95% level are reached during wintertime at a few grid points in total surface heat flux (Q_{tot}) and at none in air temperature and sea level pressure. Additionally, the mean wintertime 500-mb heights of the coupled

---

[1] The coupled simulation was integrated before the control, making it possible to prescribe climatological ocean temperatures in the North Atlantic that are identical to those in the coupled simulation. The long-term mean SST climatology of the coupled simulation is very similar to the Alexander and Mobley (1976) SST climatology in the North Atlantic.
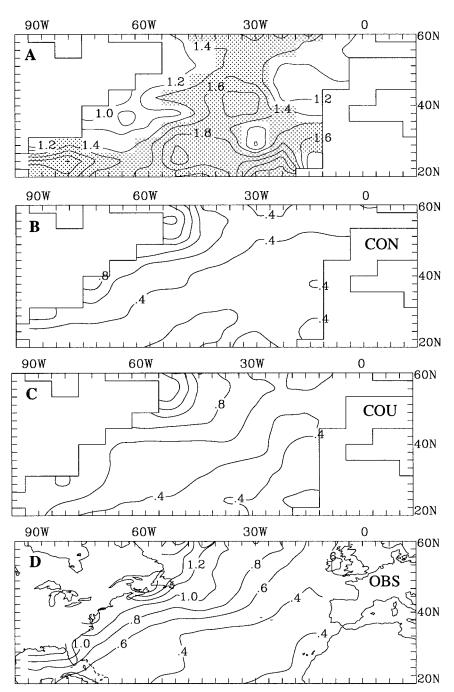
FIG. 1. The wintertime (a) ratio of coupled over control T_{air} standard deviation, and standard deviations of T_{air} from the (b) control, (c) coupled, and (d) COADS observations based on seasonally averaged DJF anomalies. The contour intervals are 0.2° in (a) and 0.2°C in (b)–(d). Shading indicates significance at the 95% or greater level using an F test.

and control simulations are not significantly different. The storm tracks, or more specifically synoptic-scale activity since both highs and lows are represented, are identified by calculating the root-mean-square (rms) of the filtered November–April 500-mb heights. The rms of daily 500-mb heights was calculated according to the technique outlined in Lau (1988), using the filter

of Raymond (1988) to isolate variations on the timescale of 2–7 days. The 31-yr averaged wintertime 500-mb heights rms in the North Atlantic sector from the coupled and the control simulations are nearly indistinguishable and are approximately 70% of the strength of the observed rms (see Fig. 1 of Lau 1988). The difference between the mean climatologies of the at-
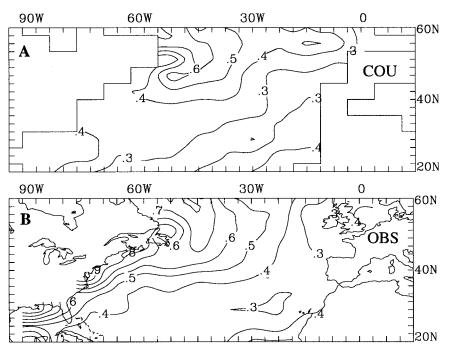
FIG. 2. Standard deviation of ocean surface temperature for (a) coupled simulation and (b) COADS observations based on seasonally averaged wintertime (DJF) anomalies. Units are in °C and the contour interval is 0.2°C.

mospheric components of coupled and control simulations in the North Atlantic Sector is not significant at the 95% level.

b. Wintertime climate anomalies

The variance of the monthly and seasonally averaged anomalies from the coupled and the control simulations is calculated. An F test (Brooks and Carruthers 1953) is used to assess the significance of the change in variance between the control and coupled simulations. The results are displayed as a ratio of coupled over control standard deviations based on seasonally averaged DJF anomalies where shading indicates significance at the 95% or greater level.

Air temperature (T_{air}) variance is enhanced in the coupled simulation during the winter season (DJF) and also for the average of November–April (not shown). Figure 1a displays the ratio of coupled over control standard deviations of air temperature. The largest values (>0.6°C) of the standard deviation of T_{air} in the control case are found close to the coast of North America (Fig. 1b), but in the coupled case (Fig. 1c) the larger values extend far from the coastline and better resemble the observations (Fig. 1d). This result suggests that an interactive ocean acts to alter the area of high variability of air temperature (T_{air}) from just near the coast to a much larger area of the ocean. In the control simulation, continental air moves over an ocean with no variability, and anomalies in air temperature are quickly damped by the fixed ocean surface temperatures. However, in the coupled simulation, continental air moves over an ocean that can respond to the atmospheric anomalies, which results in a slower damping of air temperature anomalies.

The variance of surface mixing ratio is also significantly enhanced as a result of coupling during the winter season (DJF), with the largest increases in the subtropical regions. For other atmospheric parameters, the addition of the interactive ocean has mixed effects. For example, differences in variance between the control and the coupled simulations of seasonally averaged (DJF) anomalies of surface pressure and 500-mb heights are small in the North Atlantic region.

The amplification of the air temperature is mainly due to an increase in variance at lower frequencies. For example, the standard deviation of the monthly averaged wintertime fields of air temperature, mixing ratio, and surface net heat flux for the coupled integration are quantitatively similar to those in the control integration. However, the variance in the seasonal average of these fields is significantly greater in the coupled integration than in the control integration.

Overall, the standard deviations of wintertime ocean surface temperature for DJF from the coupled simulation ocean surface temperature compare favorably (Fig. 2), and in the northern region of the ocean domain the magnitudes are only slightly weaker in the model than the observations. The standard deviations are most notably weaker than the observed near the southeastern coast of North America in the region of the Gulf Stream.
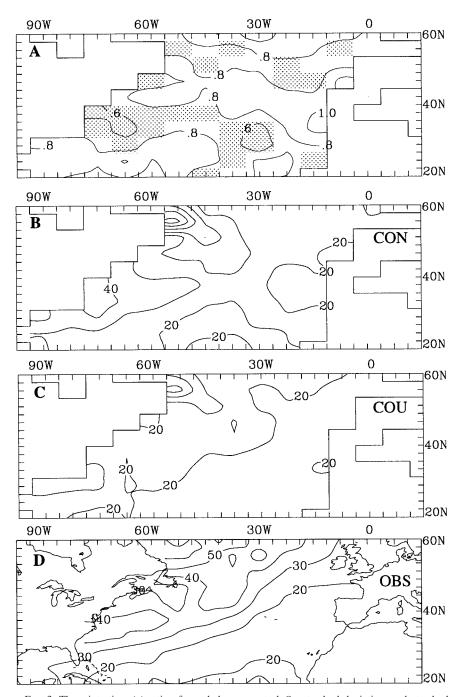
FIG. 3. The wintertime (a) ratio of coupled over control Q_{tot} standard deviation, and standard deviations of Q_{tot} from the (b) control, (c) coupled, and (d) COADS observations based on seasonally averaged DJF anomalies. Units are W m^{-2} and contour intervals are 0.2 in (a) and 10 W m^{-2} in (b)–(d). Shading indicates significance at the 95% or greater level using an F test.

The variability in the total surface heat flux (Q_{tot}) decreases with coupling over the DJF season. Figure 3a displays the ratio of coupled over control standard deviations of total surface heat flux, which is defined as the sum of the incoming solar shortwave, net outgoing longwave, sensible, and latent heat fluxes. The significant decrease in the variance of Q_{tot} is mainly due to decreases in sensible and latent heat flux variability. When the ocean temperature adjusts to the overlying atmosphere in the coupled simulation, the air–sea temperature difference is reduced, resulting in smaller heat flux anomalies and variances. Our results with a variable mixed layer depth ocean model are consistent with those of Barsugli (1995), O'Brien and

Chassignet (1996), and Saravanan and McWilliams (1998), who also find a decrease in heat flux variance with coupling. Variability of the total heat flux in the control case reaches a maximum along the coast of North America and decreases eastward (Fig. 3b). With an interactive ocean the variability of the total heat flux has decreased, particularly near the coast of North America (Fig. 3c). The variability of observed heat fluxes (Fig. 3d) was estimated by seasonally averaging the monthly mean heat fluxes calculated from COADS daily data and is larger than that from the coupled and control model integrations. The difference between the coupled model and observed heat flux variance is likely due to the model resolution and the exclusion of ocean advection in the MLM.

c. EOF analysis

Empirical orthogonal functions (EOF) over the North Atlantic sector are constructed from seasonally averaged anomalies of wintertime (DJF) air temperature for the control, coupled, and observed data. Because air temperature data are available for both the control and the coupled simulations, it has been chosen as the primary variable for this analysis. The focus of this section will be the first EOF of model air temperature, which is characterized by a north–south-oriented dipole in the western Atlantic and is similar to that from the observations (see Wallace and Jiang 1987; Cayan 1992; Deser and Blackmon 1993).

The first EOF of air temperature during DJF for the coupled, control, and observed data clearly displays a dipole pattern (Fig. 4). The EOFs in Fig. 4 are presented as correlations between the time coefficients (pc) and air temperature anomalies to highlight the amount of variance explained at each grid point by the dipole mode. Coupling does not significantly change the spatial pattern of the leading EOF from that in the control CCM1 (cf. Figs. 4a and 4b) and the first EOF from both simulations strongly resemble that from the observations (Fig. 4c). The model simulations also capture the weaker positive (north) and negative (south) patterns in the eastern part of the Atlantic that are evident in the observations. The absolute variance of coupled EOF1 is larger than the control. The total variance from EOF1 in the coupled (control) case is approximately 56% (30%) of that in EOF1 from the observations. The first mode explains 27% of the total variance in the coupled case, 43% in the control case, and 30% in the observed, indicating that coupling increases the variance in non-EOF1 patterns more than it increases it in the EOF1 pattern.

Regression coefficients of mixing ratio, total heat flux, and surface pressure on the time coefficients of EOF1 of T_{air} for the coupled simulation are consistent with the patterns of EOF1 and the observed composites discussed in Battisti et al. (1995). Anomalously cool air is associated with reduced moisture, increased heat flux from the ocean, and low surface pressure to the north of the cool air. Regression coefficients from the control simulation are close to those of the coupled integrations in the northern half of the domain. In the southern part of the domain, control regression coefficients of mixing ratio on the time coefficient of EOF1 of air temperature are nearly 60% larger than those from the coupled simulation. Changes in heat flux and pressure associated with a 1.0°C change of the time coefficient are also larger in the southern regions of the control simulation. The regression plots can be examined in section 4-4 of Bhatt (1996).

The time coefficients of the first EOF of T_{air} for the coupled, control, and observed data are presented in Fig. 5. Time coefficients from the coupled simulation (Fig. 5b) contain more variance at lower frequencies than in the control (Fig. 5a), with increased variability extending to the decadal timescale in the coupled integration. Autocorrelation of these time coefficients[2] (Fig. 6) confirm that the persistence of anomalies associated with the first EOF has increased with coupling, with the coupled autocorrelations decaying slower than those from the control. The autocorrelation of time coefficients of coupled air temperature at a 1-yr lag is significant at the 95% level. Although the coupled and control autocorrelations are not statistically different from each other at the 90% level, collectively, the evidence that we present in the following sections supports an increase in persistence of surface atmospheric anomalies with coupling. The autocorrelations of the time coefficients of EOF1 of observed air temperature (Fig. 6) display greater persistence than that in the control simulation but less persistence than in the coupled. The lag one autocorrelation of the time coefficients of observed air temperature (Fig. 6) is significant at the 90% level. The observed autocorrelations are sensitive to the period chosen, with a lag of 1-yr autocorrelation of 0.47 (0.24) if the last (first) 31 of the total 38-yr record is used in the calculation. Therefore, more realizations of the observations are needed to reduce the error bars associated with the autocorrelations.

4. Persistence in the atmosphere and ocean

a. Examination of enhanced low-frequency variability

1) AUTOCORRELATIONS

To examine the persistence of anomalies further, two indices of air temperature anomalies for all months of the year were constructed from model output and observations by averaging together monthly anomalies at several grid points located in the northern and southern

---

[2] Note that the lag is in years since the EOF is calculated using wintertime averaged (DJF) air temperature anomalies.
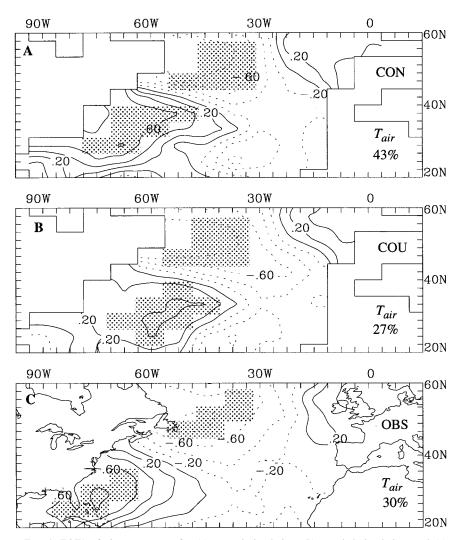
FIG. 4. EOF1 of air temperature for (a) control simulation, (b) coupled simulation, and (c) observations (COADS) for seasonal wintertime (DJF) anomalies. The maps are presented as a correlation between the time coefficient of EOF1 and air temperature anomalies. Shading denotes northern and southern regions used to calculate area average indices for autocorrelations.

centers of maximum variability of EOF1 (see shaded areas in Fig. 4). The data are averaged over slightly different grid points since the centers of maximum dipole variability are not the same in the simulations and observations. Autocorrelations starting each month were constructed for lags of 0–24 months and a 1–2–1 time filter was applied to reduce noisiness. Figures 7 and 8 display autocorrelations from lag 0 to 15 months for the indices based on the northern and southern centers of high variability, respectively. There are no significant or organized features in the autocorrelations beyond 15 months. Accounting for a reduction of the degrees of freedom due to persistence (Quenouille 1954), we find that at lags of 2–3 (9–10) months, a significance level of 95% is reached for correlations greater than 0.36 (0.42). Autocorrelations that are significantly different at the 90% level in the control and

coupled integrations are indicated by the shading in Figs. 7b and 8b.

In the coupled integrations, the autocorrelations of monthly air temperature based on the northern index between January and April of one winter and the following January stand out in Fig. 7b and are the largest autocorrelations (0.4–0.6) found at a lag of about 10–12 months. Air temperature in the control simulation (Fig. 7a) is not strongly correlated from one winter to the next. Autocorrelations of observed air temperature in the northern part of the domain (Fig. 7c) closely resemble those from the coupled simulation and display large positive values for air temperature during winter/spring with that in the following fall, 7–11 months later, supporting the re-emergence mechanism. It should be noted that the signature of re-emergence in air temperature autocorrelations closely resembles that found in
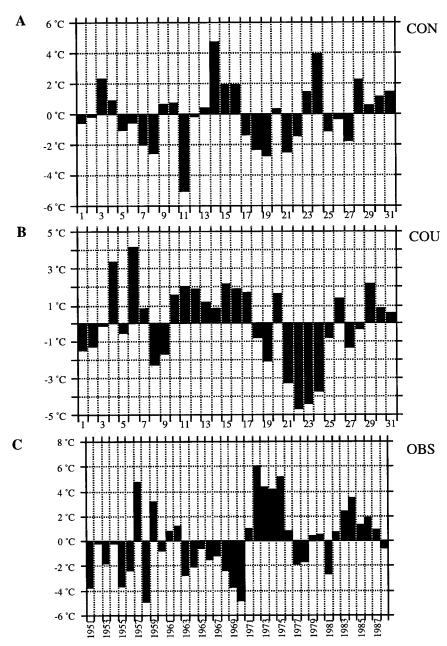
FIG. 5. Time coefficients for EOF1 of T_{air} for (a) control, (b) coupled, and (c) observations (COADS) based on seasonally averaged wintertime (DJF) anomalies. The units are °C. The year given on the x axis refers to January and February.

autocorrelations of SSTs. The maximum autocorrelation in the observed air temperatures occur earlier in the winter and are smaller in magnitude than those in the coupled simulation, suggesting that the model overrepresents this effect of the ocean memory. Processes such as advection, not included in the ocean model, would likely reduce the impact of the re-emergence mechanism, because water temperature anomalies below the mixed layer would be mixed horizontally over the course of the year, leading to weaker temperature anomalies at depth.

In the southern part of the Atlantic domain the air temperature autocorrelations from early spring to the following winter are weak and not significantly different between the control and coupled simulations (Figs. 8a and 8b). The observed autocorrelations in the southern part of the domain also display weak correlations from one winter to the next (Fig. 8c), resembling those from the coupled and control simulations.

During the summer months, the autocorrelations of air temperature are significantly greater at lags of 1–3 months in the coupled than the control simulation for
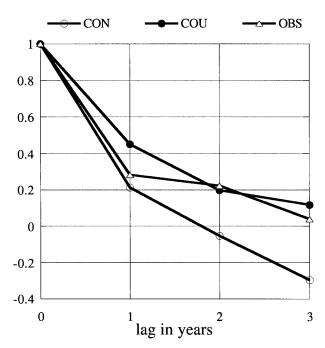
FIG. 6. Autocorrelation of the time coefficients of EOF1 (based on averaged DJF anomalies) of T_{air} from the control (open circle), the coupled (shaded circle) simulations, and the observations (open triangle). The lag 1 autocorrelation from the coupled simulation (observation) is significant at the 95% (90%) level or greater using a t test. The difference between the autocorrelations from the coupled and control simulations at a lag of 1 yr is not significant at the 90% level using the method outlined in section 13.7 of Press et al. (1990).

indices based on both the northern and southern domains (cf. values of autocorrelations along the left most solid vertical line in panels a and b of Figs. 7 and 8). Summertime autocorrelations of observed air temperature (Fig. 7c and 8c) are approximately 0.6 or greater at lags of 0–3 months in the northern part of the domain and are somewhat weaker in the southern part of the domain. Autocorrelations of monthly coupled and observed ocean temperatures (see Fig. 5-8 in Bhatt 1996) closely resemble the autocorrelations of air temperature in Figs. 7b,c and 8b,c.

It is hypothesized that in the model results the Namias–Born hypothesis plays a key role in the large autocorrelations between one winter and the next, while decreased thermal damping (Barsugli 1995) explains the important differences between the coupled and control integration on the seasonal timescale. The increase in persistence at both timescales in the context of the proposed mechanisms is examined next.

2) DECREASED DAMPING BY HEAT FLUXES

Turbulent heat fluxes act to strongly damp air temperature anomalies when the ocean temperatures do not vary (Frankignoul and Hasselmann 1977; Frankignoul 1985). In climate simulations with an interactive ocean, ocean temperatures respond to atmospheric anomalies
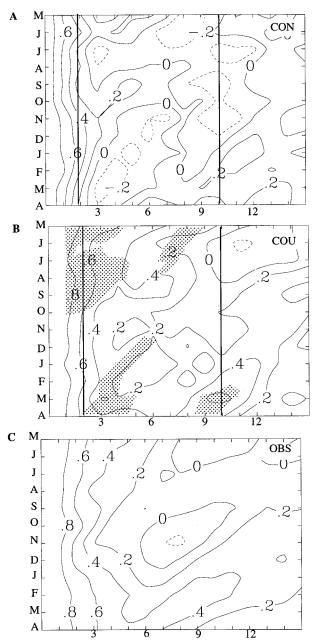

FIG. 7. Monthly autocorrelations of T_{air} in the northern part of the domain for the (a) control, (b) coupled, and (c) observed. The starting months are shown on the ordinate. At the top-left corner, the ordinate begins with the month of May and continues down the column until April. The numbers spanning from 0 to 15 on the x axis indicate the number of months after the starting month, which is given by values on the y axis. Autocorrelations greater than 0.36 (0.42) are statistically significant at the 95% or greater level at lags of 2–3 (9–10) months, as determined by Student's t-test including a reduction in the number of degrees of freedom due to persistence (Quenouille 1954). The vertical lines at 2 and 10 months highlight the monthly and interannual timescales of persistence, respectively. Shading in (b) indicates where the coupled and control autocorrelations are significantly different at the 90% level using the method outlined in section 13.7 of Press et al. (1990). Data have been smoothed using a 1–2–1 time filter prior to calculating the autocorrelations.
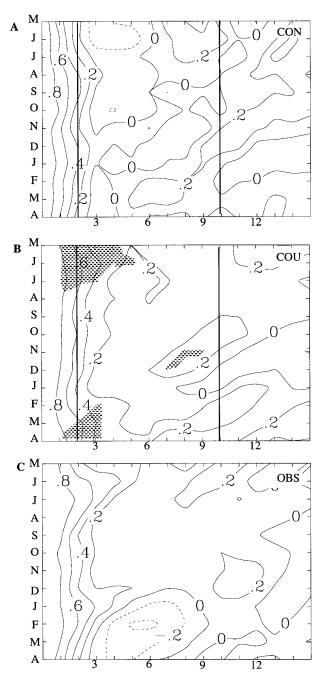
FIG. 8. Same as Fig. 7 except for the southern part of the domain.

and consequently the damping by heat fluxes of atmospheric anomalies decreases (decreased thermal damping; Barsugli 1995). Simplified sensible heat flux equations are given in Eqs. (3) and (4), for the control and coupled simulations, respectively:

$$Q_{sh} = K(T_{air} - SST),\qquad(3)$$

$$Q_{sh} = K(T_{air} - T_{mix}),\qquad(4)$$

where K is the product of air density, the specific heat

of air, transfer coefficient, and wind speed. Air temperature is represented by T_{air}, climatological sea surface temperature by SST, and ocean mixed layer temperature by T_{mix}. When the ocean is able to respond to the atmosphere, a positive anomaly of air temperature leads to a positive ocean temperature anomaly [Eq. (4)]. The sensible heat flux is proportional to the air–sea temperature difference; consequently, it will be smaller in the coupled than the uncoupled case where the SST is fixed [Eq. (3)]. The larger heat flux anomaly in the uncoupled situation will damp air temperatures faster than in the coupled case.

Autocorrelations of air temperature beginning in June and July are significantly different between the coupled and control simulations (Figs. 7 and 8) for lags of 1–4 months. In the northern domain, temperature autocorrelations at a lag of 2 months beginning in June, July, and August are approximately 0.2 in the control and between 0.6–0.8 in the coupled simulation (Fig. 7). The increase of autocorrelations is similar but slightly weaker in the south (Fig. 8). The largest increase in the autocorrelation with coupling of air temperature at lags of 1–4 months occurs for autocorrelations that begin in July. The standard deviations of seasonal June–August air temperatures are more than two times larger, while those calculated using monthly anomalies are only 1.5–2 times larger in the coupled simulation than the control. Additionally, the summertime surface heat flux variance decreases with coupling.

The increase in air temperature autocorrelations, clearly visible during the summer months, along with the increase in air temperature variance and concurrent decrease in heat flux variability resulting from coupling are consistent with decreased thermal damping (Hasselmann 1976; Frankignoul 1985; Barsugli 1995; Barsugli and Battisti 1998). This is not to say that changes in thermal damping do not operate during the winter months in this model but just that it is clearly evident in the warmer months. The analysis of winter climate anomalies in section 3 shows that seasonal (DJF) variance of air temperature increases with a concurrent decrease in heat flux variance, which is consistent with a decrease in thermal damping.

3) "RE-EMERGENCE" MECHANISM

The large autocorrelations seen from one winter to the next in the northern part of the domain for both air (Fig. 7b) and ocean temperature would be expected if the re-emergence mechanism is operating in the coupled simulation. The MLM was used in conjunction with the ocean weathership data by Alexander and Deser (1995) to demonstrate that this mechanism operates at various locations in the northern midlatitude oceans.

Lag correlations from the coupled simulation of February ocean surface temperatures with ocean temperature from the surface to a depth of 225 m support the hypothesis that the re-emergence mechanism operates
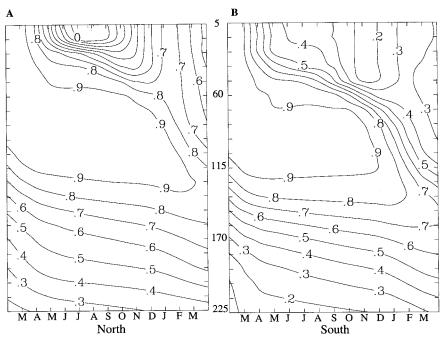
FIG. 9. Correlations between February surface ocean temperature and ocean temperatures from the surface to a depth of 225 m for the next 14 months. Correlations in the northern part of the domain are shown in (a) and in the southern part in (b). Data have been smoothed using a 1–2–1 time filter prior to calculating the autocorrelations. Autocorrelations greater than 0.36 (0.42) are statistically significant at the 95% or greater level for lags of 2–3 (9–10) months.

in the northern part of the coupled domain (Fig. 9). Autocorrelations at the surface decrease during the warm months and increase again during fall, reaching a maximum in following winter (DJF) (Figs. 9a and 9b). The surface correlations are, however, larger in the north (0.7–0.8) than in the south (0.3–0.4) the following winter (December–March). Similarly, regression coefficients of winter ocean temperature on ocean temperature for the previous February are 0.7–0.8 ($^\circ$C $^\circ$C^{-1}) in the northern and 0.2–0.3 in the southern part of the domain. The correlations begin to increase during the fall when water from below the summer thermocline is introduced back into the surface layer. Autocorrelations are largest in February when the mixed layer is deepest because a maximum amount of the ocean water from the previous winter has been reincorporated into the surface layer. The wintertime surface ocean temperature anomalies are significantly correlated with sub–mixed layer water during summer in the north and the south as seen by following the 0.9 contour line.

Lag correlations of ocean temperature from the surface to 220 m are consistent with what would be expected if re-emergence is primarily responsible for the persistence in ocean temperature anomalies seen at lags of 10–12 months in the north. In the southern part of the basin, significant autocorrelations of ocean temperature from one winter to the next do not occur in the model, consistent with the lack of memory from one

winter to the next displayed in the air temperature autocorrelations.

b. Sensitivity experiments to examine the re-emergence mechanism

A set of uncoupled experiments are presented that examine the influence of entrainment variability on the re-emergence of SST anomalies. An uncoupled control experiment is constructed by forcing the MLM with surface fluxes from the coupled simulation and two sensitivity experiments are conducted in which mixed-layer depth is specified and sub–mixed layer temperature anomalies are removed. The experiments are summarized in Table 1.

1) EXPERIMENT SETUP

The mixed layer model is forced with daily heat fluxes, wind stress, and freshwater forcing (E − P; evaporation minus precipitation) from the 31-yr coupled simulation in the one-way forced manner to construct a control simulation (TOTF). Weak damping (3-yr time-scale) in the ocean temperature tendency equation is included in all of the multiyear one-way forced simulations in order to prevent the ocean temperatures from

TABLE 1. A summary of the one-way-forced experiments that are performed to examine the impact of entrainment variability on the persistence of ocean temperature anomalies.

Experiment	Description
Total forcing (TOTF)	Forced with heat, momentum, and freshwater fluxes from the coupled simulation. T_{mix} damped with 3-yr timescale.
Fixed h_{mix} annual cycle FIXED h_{mix}	Forcing and damping from TOTF. $h'_{mix} = 0$ and $Q'_{we} = 0$.
No anomalies in T_{below} NOA T_b Aug–Dec	Forcing and damping from TOTF. T'_b set to 0 annually on 1 Aug or 1 Sep or 1 Oct or 1 Nov or 1 Dec.

drifting.[3] A damping timescale of 3 yr maintains the persistence of EOF1 of mixed layer temperature from the coupled simulation. This damping timescale is significantly weaker than 4–6 months (Frankignoul 1985), which is inferred from the observations. The spatial patterns and time coefficients of EOF1 of mixed layer

---

[3] Small changes in surface forcing can lead the model-predicted values to diverge greatly from the corresponding value in the coupled simulation.
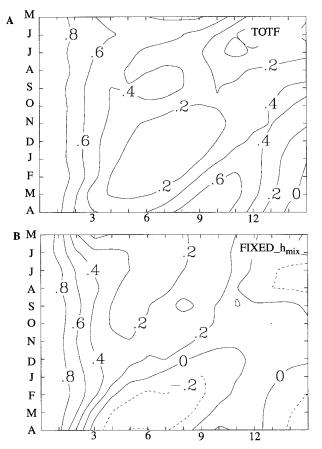

FIG. 10. Autocorrelations of T_{mix} averaged over the northern grid points centered at the maximum variance for the dipole mode of variability for experiments (a) TOTF and (b) FIXED h_{mix} at monthly lags of 0–15. Data have been smoothed using a 1–2–1 time filter prior to calculating the autocorrelations.

temperature in the coupled and the TOTF simulations compare favorably. The pattern correlation is 0.94 and the temporal correlation is 0.86. In the sensitivity experiments, the surface forcing and ocean temperature damping are identical to the TOTF simulation, but the strength of entrainment is varied.

2) SENSITIVITY EXPERIMENT RESULTS

In the northern domain (as defined by the shaded region in Fig. 4), monthly autocorrelations of mixed layer temperature from the TOTF (Fig. 10a) simulation display a structure similar to that of autocorrelations of coupled air temperature (Fig. 7b). The correlations between March and April ocean mixed layer temperature and the temperature 9–10 months later are larger than 0.6. Similarly, observed autocorrelations (Fig. 5-8c in Bhatt 1996) between late winter SST and SST 6–12 months later reach a maximum value of 0.6. The winter-to-winter correlations that are attributed to the re-emergence mechanism are evident in the ocean temperature autocorrelations.

In the first sensitivity experiment (FIXED h_{mix}), the model is forced with the same surface fluxes and damping as the TOTF case. In addition, the annual cycle of mixed layer depth and mean heating due to entrainment (Q_{we}) are specified to be the climatological values from the control experiment (TOTF), which ensures that there are no anomalies in entrainment heating (Q'_{we}) or mass flux as well as h_{mix}. The mixed layer temperatures in FIXED h_{mix} drifted and were detrended prior to analysis.

When the annual cycle of mixed layer depth is specified (FIXED h_{mix}), the strong autocorrelations between March SST and that 8–10 months later seen in TOTF (Fig. 10a) are not present (Fig. 10b). This is expected if re-emergence is responsible for the strong autocorrelations since water from the previous winter must be reincorporated into the mixed layer in the fall. Additionally, the autocorrelations 3–9 months after winter are weakly negative (Fig. 10b), suggesting that mixed layer temperatures become decorrelated in less than 3 months.

In the next sensitivity experiment (NOA T_b), the model is integrated with the same surface fluxes and damping as the TOTF case but the temperature below the mixed layer is reset to the climatological mean profile on the first of August each year (NOA T_b Aug). We
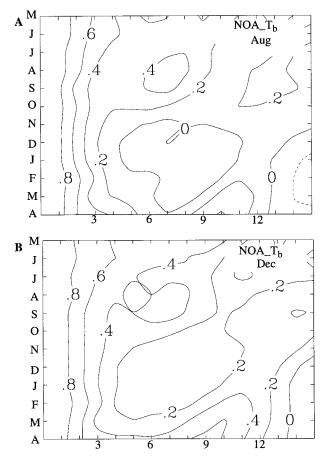
FIG. 11. Monthly autocorrelations of T_{mix} in the north for (a) NOA T_b Aug and (b) NOA T_b Dec. The starting months are shown on the ordinate. Data have been smoothed using a 1–2–1 time filter prior to calculating the autocorrelations.

repeated this experiment several times, resetting the subsurface temperature profile to climatological values on the first day of September, October, November, and December (NOA T_b Sep–Dec). In these experiments, T_b' is set to zero in Eqs. (1) and (2). During August the mixed layer is relatively shallow and by resetting all sub–mixed anomalies to zero there is no carry over of sub–mixed-layer temperature anomalies from one winter to the next. The autocorrelations of mixed layer temperature starting at each calendar month (Fig. 11, only NOA T_b Aug and Dec shown) indicate that the autocorrelation between one winter and the next gets larger as the reset date of the subsurface temperature anomalies is delayed. The autocorrelation patterns progress smoothly between Figs. 11a and 11b for the months between August and December (see Fig. 5-25, Bhatt 1996). When the subsurface anomalies are reset on the first of December the mixed layer temperature autocorrelations (Fig. 11) between one winter and the next are slightly weaker than those from TOTF (Fig. 10a).

In summary, limiting the variability of entrainment in the MLM, whether by setting subsurface anomalies

to zero or by specifying climatological values of heating due to entrainment and mixed layer depths, has had the most notable effect of reducing the autocorrelations of mixed layer temperatures from one winter to the next in the northern part of the domain. These experiments suggest that the persistence of mixed layer temperature anomalies from one winter to the next strongly depends on the history of sub–mixed layer temperature anomalies and how these anomalies interact with water in the surface layer.

c. Discussion

The CCM1 coupled atmospheric variability strongly favors a carryover of climate anomalies from one winter to the next, and there is a weak hint of this in the control simulation. In the control simulation, the autocorrelations of the time coefficients of EOF1 of air temperature at a lag of one year (Fig. 6), surface heat flux (Fig. 5-16a in Bhatt 1996), and the largest autocorrelations of air temperature from one winter to the next in the northern part of the domain are weakly positive (slightly greater than 0.2). Climate models integrated with specified annual cycle of SSTs have been shown to exhibit variability at much longer timescales (James and James 1989; M. Hoerling 1997, personal communication), which has been attributed to the nonlinear dynamics of the atmospheric flow (James and James 1989). While there is some weak low-frequency variability in the control simulation, the timescale of anomalies is significantly enhanced by including air–sea interaction.

Curiously, the re-emergence of mixed layer temperature anomalies from one winter to the next is prominent in the northern part of the domain and not seen in the southern part of the domain in both the coupled simulation and the observations. It was believed that a heat budget analysis similar to Alexander and Penland (1997) would clearly explain the differences between the north and the south. Unfortunately, the partitioning of the heat budget did not clearly indicate that the mean entrainment of the anomalous temperature jump across the mixed layer played a larger role in the north than the south. Other factors, such as the stronger vertical temperature gradient in the south, need to be explored further to better understand the difference between the north and the south in the model. Recent observational analysis of expendable bathothermograph data in the North Atlantic (M. Alexander, C. Deser, and M. Timlin 1997, personal communication) suggests that the geographical dependence of re-emergence is very sensitive to the time period used in the analysis. Therefore the similarity between the model and observations may be fortuitous.

The re-emergence effect is overrepresented in this model as evidenced by the stronger autocorrelations of air temperature (Figs. 6 and 7b,c) and SST (see Figs. 5-8a and 5-8c in Bhatt 1996) in the coupled case than in the observations. This is not surprising since there is
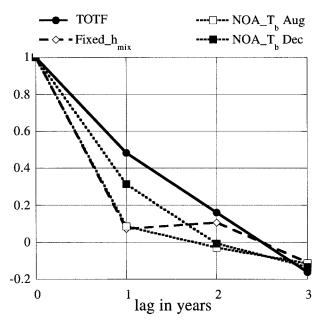
FIG. 12. Autocorrelations of T_{mix} from the series of one-way-forced sensitivity experiments: full forcing (shaded circle), Fixed h_{mix} (open diamond), NOA T_b reset on 1 August (open square), and NOA T_b reset on 1 December (shaded square). Autocorrelations at a lag of 1 yr are very weak when temperature anomalies in the sub–mixed layer are suppressed.

no lateral movement of the subsurface or surface thermal structure because the mixed layer ocean model does not include advection. Also note that the subsurface temperature autocorrelations shown in Fig. 9 are significantly stronger than similar lag correlations of observed ocean temperature shown in Fig. 5 of Alexander and Deser (1993). Our results must be viewed keeping in mind that the interannual persistence of anomalies will be weaker in a model with advection.

The model results suggest that decreased thermal damping is important for mixed layer temperature variability within a season. However, on interannual timescales in this model the re-emergence mechanism plays a more pronounced role than decreased thermal damping. In the one-way-forced sensitivity experiments, the impact of decreased thermal damping, which is set by the coupled forcing terms, should not change in the sensitivity experiments. Autocorrelations at yearly lags of wintertime (DJF) mixed layer temperature from sensitivity experiments (Fig. 12) are near zero at a lag of one year. Since the sensitivity experiments limit the role of entrainment (i.e., re-emergence), then if decreased thermal damping was important on interannual timescales, then the lag 1-yr autocorrelations of SST should not drop to nearly zero in the FIXED h_{mix} or NOA T_b Aug experiments. This suggests that thermal damping is a weaker effect than re-emergence from one winter to the next and is likely more important on shorter timescales.

5. Summary

The role of midlatitude air–sea interaction on Atlantic climate variability is examined using a mixed layer model of the North Atlantic Ocean (20°–60°N) and the NCAR atmospheric GCM, CCM1. This research focuses on the impact of air–sea interaction on the natural variability of monthly to interannual timescales with an emphasis on interannual variability in the lower atmosphere during the fall and winter months of September–March.

The CCM1 is coupled to the MLM in the North Atlantic and integrated for 31 yr. The annual cycle of SSTs is specified according to the observed climatology of Alexander and Mobley (1976) outside of the North Atlantic basin. A parallel 31-yr-long control simulation of CCM1 is integrated using as a lower boundary condition the globally specified climatological annual cycle of sea surface temperatures of the coupled simulation. The primary mode of observed interannual variability in the North Atlantic is characterized by a north–south-oriented dipole in surface air temperature and ocean temperature (e.g., Wallace and Jiang 1987) and is reproduced in both the control and coupled integrations. Coupling does not quantitatively change the structure of the patterns of atmospheric variability over the midlatitude North Atlantic. In this study, we find that an interactive midlatitude North Atlantic leads to an increase in the low-frequency variability of near-surface air temperature on monthly and interannual timescales. For example, on monthly (interannual) timescales, the ratio of coupled to uncoupled wintertime (DJF) surface air temperature variance averaged over the North Atlantic is 1.3 (1.5).

Significant autocorrelations (at the 95% level or greater) of air and ocean temperature are found between one winter and the following winter in the northern part of the domain of the coupled simulation. The persistence of anomalies from one winter to the next is found to be consistent with re-emergence mechanism (Namias and Born 1970, 1974; Alexander and Deser 1995). In late winter (February–March) ocean temperature anomalies penetrate to great depths when the ocean mixed layers are at their annual maximum. During summer the mixed layer reforms closer to the ocean surface and the wintertime temperature anomalies are sequestered below the shallow summer mixed layer. These anomalies re-emerge into the mixed layer the following fall when the mixed layer begins to deepen. An analysis of sub–mixed layer ocean temperature anomalies in the northern part of the basin indicates that February mixed layer temperatures are uncorrelated with ocean surface temperatures but are strongly correlated (0.9) with temperatures between 50 and 120 m during the following summer, suggesting that temperature anomalies are sequestrated below the summer mixed layer. Uncoupled sensitivity experiments indicate that when temperature anomalies below the mixed layer are eliminated, then the persistence of anomalies from one winter to the next

is very weak. This also suggests that the re-emergence mechanism operates in the coupled simulation to yield strong autocorrelations on the interannual timescale.

Autocorrelations of air temperature at lags of 1–3 months are significantly greater as a result of coupling; this is especially evident at all times of the year in the southern half of the North Atlantic domain but is also clear during summer in the model's North Atlantic. The increased persistence on these shorter timescales is attributed to a decrease in thermal damping (Barsugli 1995). There is a statistically significant increase in the variance of seasonal wintertime (DJF) surface air temperatures and a decrease (by factor of 1.66) in the variance of surface heat fluxes with coupling. When the ocean is able to adjust to the overlying atmosphere, the negative feedback effect of heat fluxes is decreased, which is consistent with the changes in seasonal air temperature and heat flux variance.

In summary, the impact of air–sea interaction on climate variability in the midlatitude North Atlantic can be described as follows. The spatial scale of the dipole mode of variability is determined by the atmosphere, and the integrated effects of the atmospheric forcing result in a lower-frequency response in the ocean. The feedback of the ocean on the atmosphere is subtle and alters the variance and persistence of the atmospheric dipole anomalies. The role of anomalous entrainment overall acts to enhance the dipole mode of variability in SST anomalies, particularly in the northern part of the domain. Hence, the model results suggest that both re-emergence and thermal damping play important roles in midlatitude climate variability.

The present paper has focused on variability in the near-surface layer of the atmosphere and the ocean mixed layer. Ongoing analysis of the differences in the upper atmosphere associated with coupling suggest that the patterns of natural variability over Europe of 500-mb height are somewhat modified by the coupling: they more closely resemble the atmospheric response to imposed midlatitude forcing found in Palmer and Sun (1985) and Peng et al. (1995). Further examination is necessary to confirm whether these differences in patterns over Europe are statistically significant.

REFERENCES

Adamec, D., R. L. Elsberry, R. W. Garwood, and R. L. Haney, 1981: An embedded mixed-layer ocean circulation model. *Dyn. Atmos. Oceans,* **6,** 69–96.

Alexander, M. A., 1990a: Simulation of the response of the North Pacific Ocean to the anomalous atmospheric circulation associated with El Niño. *Climate Dyn.,* **5,** 53–65.
——, 1990b: Midlatitude air–sea interaction in the North Pacific. Ph.D. dissertation, University of Wisconsin—Madison, 150 pp. [Available from Center for Climate Research, Dept. of Atmospheric and Oceanic Sciences, University of Wisconsin—Madison, 1225 W. Dayton St., Madison, WI 53706.]
——, and C. Deser, 1995: A mechanism for the recurrence of wintertime midlatitude SST anomalies. *J. Phys. Oceanogr.,* **25,** 122–137.
——, and C. Penland, 1997: Variability of a mixed layer ocean model driven by stochastic atmospheric forcing. *J. Climate,* **10,** 2424–2442.
Alexander, R. C., and R. L. Mobley, 1976: Monthly average sea–surface temperatures and ice-pack limits on a 1° global grid. *Mon. Wea. Rev.,* **104,** 143–148.
Barsugli, J. J., 1995: Idealized models of intrinsic midlatitude atmosphere–ocean interaction. Ph.D. dissertation, University of Washington, 189 pp. [Available online from http://www.cdc.noaa.gov/~jjb/thesis.html.]
——, and D. S. Battisti, 1998: The basic effects of atmosphere–ocean thermal coupling on midlatitude variability. *J. Atmos. Sci.,* **55,** 477–493.
Battisti, D. S., U. S. Bhatt, and M. A. Alexander, 1995: A modeling study of the interannual variability in the wintertime North Atlantic Ocean. *J. Climate,* **8,** 3067–3083.
Bhatt, U. S., 1996: Role of atmosphere–ocean interaction in the midlatitude north Atlantic on climate variability. Ph.D. dissertation, University of Wisconsin, 159 pp. [Available on-line from http://www.mindspring.com/~bhattman/ThesisTOC.html].
Bjerknes, J., 1962: Synoptic survey of the interaction of sea and atmosphere in the North Atlantic. Vilhelm Bjerknes Centenary volume. *Geophys. Publ.,* **24,** 115–145.
——, 1964: Atlantic air–sea interaction. *Advances in Geophysics,* Vol. 20, Academic Press, 1–82.
Bladé, I., 1997: The influence of midlatitude ocean/atmosphere coupling on the low-frequency variability of a GCM. Part I: No tropical SST forcing. *J. Climate,* **10,** 2087–2106.
Brooks, C. E. P., and N. Carruthers, 1953: *Handbook of Statistical Methods in Meteorology.* AMS Press, 412 pp.
Cayan, D., 1992: Latent and sensible heat flux anomalies over the northern oceans: Driving the sea surface temperature. *J. Phys. Oceanogr.,* **22,** 859–881.
Deardorff, J., 1972: Parameterization of the planetary boundary layer for use in general circulation models. *Mon. Wea. Rev.,* **100,** 93–106.
Delworth, T., 1996: North Atlantic interannual variability in a coupled ocean–atmosphere model. *J. Climate,* **9,** 2356–2375.
Deser, C., and M. L. Blackmon, 1993: Surface climate variations over the North Atlantic Ocean during winter: 1900–89. *J. Climate,* **6,** 1743–1753.
Ferranti, L., F. Molteni, and T. N. Palmer, 1994: Impact of localized tropical and extratropical SST anomalies in ensembles of seasonal GCM integrations. *Quart. J. Roy. Meteor. Soc.,* **120,** 1613–1645.
Frankignoul, C., 1985: Sea surface temperature anomalies, planetary waves, and air–sea feedback in the middle latitudes. *Rev. Geophys.,* **23,** 357–390.
——, and K. Hasselmann, 1977: Stochastic climate models. Part 2: Application to sea–surface temperature anomalies and thermocline variability. *Tellus,* **29,** 284–305.
——, and R. W. Reynolds, 1983: Testing a dynamical model for midlatitude sea surface temperature anomalies. *J. Phys. Oceanogr.,* **13,** 1131–1145.
Gallimore, R. G., 1995: Simulated ocean–atmosphere interaction in the North Pacific from a GCM coupled to a constant-depth mixed layer. *J. Climate,* **8,** 1721–1737.
Gaspar, P., 1988: Modeling the seasonal cycle of the upper ocean. *J. Phys. Oceanogr.,* **18,** 161–180.

Haney, R. L., 1985: Midlatitude sea surface temperature anomalies: A numerical hindcast. *J. Phys. Oceanogr.,* **15,** 787–799.

Hasselmann, K., 1976: Stochastic climate models. Part I: Theory. *Tellus,* **28,** 473–485.

James, I. N., and P. M. James, 1989: Ultra-low-frequency variability in a simple atmospheric circulation model. *Nature,* **342,** 53–55.

Kiehl, J. T., R. J. Wolski, B. P. Briegleb, and V. Ramanathan, 1987: Documentation of radiation and cloud routines in the NCAR Community Climate Model (CCM1). NCAR Tech. Note NCAR/TN-288+IA, 81 pp. [Available from NCAR, P. O. Box 3000, Boulder, CO 80307.]

Kushnir, Y., 1994: Interdecadal variations in North Atlantic sea surface temperature and associated atmospheric conditions. *J. Climate,* **7,** 141–157.

——, and N.-C. Lau, 1992: The general circulation model response to a North Pacific SST anomaly: Dependence on time scale and pattern polarity. *J. Climate,* **5,** 271–283.

Lau, N.-C., 1988: Variability of the observed midlatitude storm tracks in relation to low-frequency changes in circulation pattern. *J. Atmos. Sci.,* **45,** 2718–2743.

——, and M. J. Nath, 1996: The role of the ''atmospheric bridge'' in linking tropical Pacific ENSO events to extratropical SST anomalies. *J. Climate,* **9,** 2036–2057.

Luksch, U., 1996: Simulation of North Atlantic low-frequency SST variability. *J. Climate,* **9,** 2083–2092.

Manabe, S., and R. J. Stouffer, 1996: Low-frequency variability of surface air temperature in a 1000-year integration of a coupled atmosphere–ocean–land surface model. *J. Climate,* **9,** 376–393.

Namias, J., and R. M. Born, 1970: Temporal coherence in North Pacific sea-surface temperatures. *J. Geophys. Res.,* **75,** 5952–5955.

——, and ——, 1974: Further studies of temporal coherence in North Pacific sea surface temperatures. *J. Geophys. Res.,* **79,** 797–798.

O'Brien, E. W., and E. P. Chassignet, 1996: Extratropical large-scale air–sea interaction in a coupled and uncoupled ocean–atmosphere model. *Climate Dyn.,* **12,** 53–65.

Palmer, T. N., and Z. Sun, 1985: A modelling and observational study of the relationship between sea surface temperature in the north–west Atlantic and the atmospheric general circulation. *Quart. J. Roy. Meteor. Soc.,* **111,** 947–975.

Paulson, C. A., and J. J. Simpson, 1977: Irradiance measurements in the upper ocean. *J. Phys. Oceanogr.,* **7,** 952–956.

Peng, S., L. Mysak, H. Ritchie, J. Derome, and B. Dugas, 1995: On the difference between early and middle winter atmospheric responses to sea surface temperature anomalies in the northwest Atlantic. *J. Climate,* **8,** 137–157.

——, W. A. Robinson, M. P. Hoerling, 1997: The modeled atmospheric response to midlatitude SST anomalies and its dependence on background circulation states. *J. Climate,* **10,** 971–987.

Pitcher, E. J., M. L. Blackmon, G. T. Bates, and S. Muñoz, 1988: The effect of North Pacific sea surface temperature anomalies on the January climate of a general circulation model. *J. Atmos. Sci.,* **45,** 173–188.

Press, W. H., B. P. Flannery, S. A. Teukolsky, and W. T. Vetterling, 1990: *Numerical Recipes: The Art of Scientific Computing.* Cambridge University Press, 702 pp.

Quenouille, M., 1954: *Associated Measurements.* Butterworths, 242 pp.

Raymond, W., 1988: High-order, low-pass implicit tangent filters for use in finite area calculations. *Mon. Wea. Rev.,* **116,** 2132–2141.

Saravanan, R., 1998: Atmospheric low frequency variability and its relationship to midlatitude SST variability: Studies using the NCAR Climate System Model. *J. Climate,* **11,** 1388–1406.

——, and J. C. McWilliams, 1998: Advective ocean–atmosphere interaction: An analytical stochastic model with implications for decadal variability. *J. Climate,* **11,** 165–188.

Wallace, J. M., and Q. Jiang, 1987: On the observed structure of the interannual variation of the atmosphere/ocean climate system. *Atmospheric and Oceanic Variability,* H. Cattle, Ed., Roy. Meteor. Soc., 17–43.

——, C. Smith, and Q. Jiang, 1990: Spatial patterns of atmosphere–ocean interaction in the northern winter. *J. Climate,* **3,** 990–998.

——, ——, and C. S. Bretherton, 1992: Singular value decomposition of wintertime sea surface temperature and 500-mb height anomalies. *J. Climate,* **5,** 561–576.

White, W. B., and A. E. Walker, 1974: Time and depth scales of anomalous subsurface temperature at ocean weather stations P, N, and V in the North Pacific. *J. Geophys. Res.,* **79,** 4517–4522.

Zorita, E., V. V. Kharin, and H. von Storch, 1992: The atmospheric circulation and sea surface temperature in the North Atlantic area in winter: Their interaction and relevance for Iberian precipitation. *J. Climate,* **5,** 1097–1108.